A novel strategy to reveal the cause of spontaneous abortion in human embryonic stages from a large embryo collection (Kyoto Collection)

Tohoru Kanahashi[1], Shigehito Yamada[1,2], Mire Tanaka[1], Ayumi Hirose[1], Chigako Uwabe[2], Katsumi Kose[3], Akio Yoneyama[4], Tohoru Takeda[5], Tetsuya Takakuwa[1]

[1]Human Health Science, [2]Congenital Anomaly Research Center, Graduate School of Medicine, Kyoto University, Kyoto 606-8507, 2606-8501, Japan

[3]Institute of Applied Physics, University of Tsukuba, Ibaragi 305-8573, Japan

[4]Central Research Laboratory, Hitachi, Ltd., Hatoyama, Saitama 350-0395, Japan

[5]Allied Health Sciences, Kitasato University, Kanagawa 252-0373, Japan

Corresponding author: Dr. Tetsuya Takakuwa

Tel/Fax: +81-75-751-3931; E-mail: tez@hs.med.kyoto-u.ac.jp

Running title

Research of miscarriage in embryonic stages

Corresponding author; Dr. Tetsuya Takakuwa

Human Health Science, Graduate School of Medicine, Kyoto University

606-8507 Sakyo-ku, Shogoin Kawahara-cyo 53, Kyoto, Japan

Grant Support

This study was supported by Grant Nos. 22591199, 24790195, 24119002, and 25461642 from the Japan Society for the Promotion of Science.

This work has been performed under the approval of the Photon Factory Program Advisory Committee (Proposal Nos. 2013G514 and 2012G138).

Abstracts

The cause of spontaneous abortion of normal conceptuses remains unknown in most cases. We aimed to reveal the cause of spontaneous abortion by using a large collection of embryo images (Kyoto collection) from a magnetic resonance imaging (MRI) database and novel phase-contrast radiographic computed tomography (PXCT). MRI data from 1,156 embryos between Carnegie stage (CS) 14 and CS23 from the Kyoto collection were screened by using the volume of the liver as the target organ. Embryos with liver volumes ≥ 2 SD above or below the mean for the stage of development were examined precisely on MRI. Embryos with potentially abnormal livers were further analyzed by using PXCT. Liver abnormality was detected in all 7 embryos in the extra-small liver group (SG) and in 2 of 8 embryos in the extra-large liver group (LG). The abnormalities in the SG consisted of hepatic agenesis (2 embryos), hepatic hypogenesis (4), and liver lobe defect (1). Among the 7 SG embryos, 2 had only liver abnormalities and 5 exhibited complications in other organs. Of the 2 LG embryos, one had only a single liver abnormality and the other had a morphologically abnormal liver with complications in other organs. Most of such liver abnormality cases are not survive,

as liver function becomes essential. The prevalence of liver malformations in CS18 and CS21 in the intrauterine population of externally normal embryos is approximately 1.7%. The present study is a first step toward the elucidation of the causes of spontaneous abortion in externally normal embryos.

Keywords

magnetic resonance imaging; phase-contrast radiographic computed tomography; human development; spontaneous abortion; intrauterine death; congenital anomaly

Abbreviations

two-dimensional (2-D); three-dimensional (3-D); common hepatic vein (CHV); Carnegie stage (CS); ductus venosus (DV); hepatic vein (HV); extra-large liver group (LG); magnetic resonance (MR); magnetic resonance microscopy (MRM); phase-contrast X-ray computed tomography (PXCT); portal sinus (PS); portal vein (PV); standard deviation (SD); extra-small liver group (SG); series of liver malformations (SLMs); umbilical vein (UV).

Introduction

Abortion is the termination of pregnancy by the removal or expulsion of a fetus or embryo from the uterus prior to viability. Most spontaneous embryonic abortions occur during the first 3 weeks. Generally, 15–20% of verified pregnancies that survive the first 4 postovulatory weeks are lost through spontaneous abortion (O'Rahilly and Müller, 2001). Identifying the cause of such spontaneous abortion from prenatal, perinatal, and maternal medical causes is certainly important. However, the cause of spontaneous abortion of normal conceptuses remains unknown in most cases because of several difficulties.

The detailed observations of embryos in utero are still limited despite the recent advent of imaging techniques such as sonography. Moreover, intact human embryos are difficult to collect after abortion. Furthermore, internal abnormalities in such small specimens are extremely difficult to diagnose both in utero and ex utero. Many factors are involved in the termination of pregnancy, not only the embryonic factor itself but also maternal health and placental conditions. Many modulators such as nutrition, poison and drug use, locomotion and injury, and infection affect intrauterine environment. Such unspecified modulation distracts attention from the laborious

inspection of embryos, especially when embryos are externally normal.

The Kyoto Collection of Human Embryos was initiated to investigate both normal and abnormal human development (Nishimura 1968). More than 40,000 embryo and fetal specimens were collected mostly between the 1960s and 1970s in Japan (Kameda et al, 2012; Shiota et al, 2007). In most cases, pregnancy was terminated during the first trimester for socioeconomic reasons under the Maternity Protection Law of Japan. The embryo population is assumed to be representative of the unselected intrauterine population in Japan (Nishimura 1974; Nishimura 1975). The collections comprised both externally normal (approximately 92%) and abnormal specimens (approximately 8%) in total (Kameda et al 2012). Life-table estimates for normal and abnormal human conceptuses showed that more than 10% of all embryos recognizable at 5 weeks' gestation (approximately Carnegie stage [CS] 12 and CS14) are malformed (Shiota, 1991). Because of selective intrauterine death of malformed embryos and fetuses, the proportion of malformed fetuses decreased to 2.4% by age 8 weeks (approximately CS21 and CS23) and to 1% at term. The cumulative intrauterine mortality rate of malformed conceptuses was estimated to be 93%. A higher incidence of spontaneous

abortion of fetuses with neural tube defects, cleft lip, and cleft palate was noted among malformed embryos, and many other malformations may be involved in the causes of spontaneous abortion. The much higher frequency of various malformations in spontaneous abortuses than in newborn babies is evidence that many abnormal human conceptuses are screened prenatally. Meanwhile, the cumulative intrauterine mortality rate in normal conceptuses was 18%. The causes of the abortion in this population are totally unclear.

The magnetic resonance microscopy (MRM) imaging database of approximately 1200 well-preserved human embryos at CS13 to CS23, diagnosed as externally normal, were acquired in 2000–2005 (the Kyoto embryo visualizing project; Shiota et al, 2007, http://atlas.cac.med. kyoto-u.ac.jp). The main purpose of the project was to observe a number of normal human embryos. Three of the coauthors (UC, SY, and KK) were involved in the projects, in depth. We have reported the three-dimensional (3-D) morphology and quantitative morphometry of various organs, such as the liver, ear, stomach, and brain, by using the database (Hirose et al., 2012; Kagurasho et al., 2012; Nakashima et al., 2012; Shiraishi et al., 2013; Kaigai. et al,

2014; Yamada et al., 2010). Such reports proved that the database is useful for research purposes and as teaching materials.

Although the magnetic resonance (MR) image database includes only externally normal embryo specimens, whether the internal organs were also normal cannot be guaranteed. Considering that the cumulative intrauterine mortality rate in normal conceptuses was estimated at 18%, the MRI database includes embryos that have potential abnormalities that lead to spontaneous abortion and/or intrauterine death. Thus, the detailed observation of the internal organs of embryo specimens from the database may provide a clue for the spontaneous abortion in the embryonic and fetal periods. In this connection, we planned to determine the cause of spontaneous abortion and/or intrauterine death by using a large embryo collection (Kyoto collection) obtained from a MRI database and novel phase-contrast radiographic computed tomography (PXCT; Figure 1) (Yoneyama et al, 2006, 2011). We chose the liver as the target organ for screening. The present data provide a novel series of liver malformations (SLMs) that would potentially cause spontaneous abortion and/or intrauterine death. This strategy will help reveal the cause of spontaneous abortions and/or intrauterine death.

Materials and Methods

MR image datasets (Kyoto embryo visualizing project)

We used 1,156 MR image datasets at CS14 to CS23. The number of cases for each CS ranged from 54 to 147. The embryos were selected as externally normal embryos from the Kyoto collection. The conditions used to acquire the MR images of the embryos have been described elsewhere (Shiota et al., 2007; Matsuda et al., 2003; Yamada et al., 2010). The 3-D MR image datasets for each embryo were initially obtained from 256 × 256 × 512 voxels. Each dataset was first converted into a two-dimensional (2-D) stack and saved in the audio-video interleave (.avi) file format by using the Image J version 1.42q software (National Institutes of Health, Bethesda, MD). Sequential 2-D images were resectioned digitally, and 3-D images were reconstructed by using the OsiriX version 3.7.1 software (Pixmeo SARL, Geneva, Switzerland). The size of each liver was measured on the 3-D image by using OsiriX, and then the liver volume was estimated.

Screening for potential liver abnormalities by estimation of liver volume

The manually segmented liver volume of 30 randomly chosen embryos was measured by manual segmentation of the liver section on sequential 2-D images obtained by using OsiriX. The dimensions of the liver in the respective 3-D directions Lx, Ly, and Lz were measured, and then the following calculation formula was assumed to estimate the liver volume from the length measurement obtained from the MR image data:

$$\text{Liver volume} = 0.373 \times Lx \times Ly \times Lz + 0.231$$

The equation was validated with another 30 randomly chosen embryos (data not shown), which were confirmed to fit ($R = 0.99$).

All embryos were then screened by using the calculation formula (Figure 1); that is, the embryos for which V was more than 2 standard deviations (SD) greater or less than the mean for the developmental stage were selected as having extra-large and extra-small livers, respectively. The selected embryos were reviewed precisely by using serial MR and 3-D reconstructed images. The 3-D images of the intrathoracic,

retroperitoneal, and intra-abdominal organs were reconstructed by using the Amira software (ver. 5.4.5, Visage Imaging, Berlin, Germany). The embryos with potential liver abnormalities were further viewed precisely by using PXCT imaging data.

Phase-contrast PXCT

The 3-D PXCT images of the human embryos were obtained by using a radiographic imaging system (BL14-C, 17.8 keV) from Photon Factory, Institute of Materials Structure Science, High Energy Accelerator Research Organization (KEK, Tsukuba, Japan). The data provide a resolution of 18 μm/pixel or better. The mechanism and conditions used to acquire the PXCT images of the embryos have been described elsewhere (Yoneyama et al., 2011).

Results

Estimation of liver volume and screening for potential liver abnormalities

The liver volume was estimated for each of 1,156 embryos (Fig. 2A). The volume was observed to increase exponentially during development.

A total of 41 cases ranging from CS14 to CS23 were selected for having liver volume values greater than the mean +2SD (extra-large) (Fig. 2B). Another 12 cases, ranging from CS19 to CS21, were selected for having liver volume values less than the mean − 2SD (extra-small) (Fig. 2B). The selected embryos were analyzed morphologically using serial MR and 3-D reconstructed images. Seven embryos in the extra-small liver volume group at CS20 and CS21 and 8 embryos in the extra-large liver volume group at CS17 and CS19 were selected as having possible liver abnormalities. The embryos were subjected to PCT analysis for diagnosis of the abnormalities. The embryos with possible liver abnormalities were classified as the extra-small liver group (SG) and the extra-large liver group (LG). No obvious morphological abnormality was observed in the MR imaging data from the remaining cases (data not shown).

The following section first describes the exact findings in each case, both within the liver (Table 1) and the complications in organs other than the liver (Table 2).

Liver morphological structure in the embryos with a small liver

Apparent abnormality of the liver was detected in all 7 embryos with a small liver. Of the 7 embryos, 2 (SG1 and SG2) were at CS20 and 5 (SG3–SG7) were at CS21. Two of the cases (SG6 and SG7) at CS21 had no liver detectable using PCT. The deviation from the mean volume ranged from −3.6SD to −2.2SD. Among the 7 SG embryos, 2 had abnormality only of the liver and 5 had complications in other organs.

In SG1 (−2.9SD, CS20), the position and morphological structure of the liver were maintained on the left side of the UV but were abruptly absent on the right side. The surface of the liver was smooth on the left side but irregular on the right side (Fig. 3A). The internal structure was malformed, and the components of the liver were poorly integrated and only loosely connected beneath the surface on the right side (* in Fig. 3B). The UV was flattened transversely at its entrance into the liver. The vascular structures of the UV, DV, and PV within the liver were apparent in the plane section (Fig. 3B). The intrahepatic regions of the UV were severely flattened and deformed (* in Fig. 3A). The PV system, including the portal sinus (PS), main branches, and sub-branches, was detected as well as in the control (Fig. 3B). The 2 terminal HVs, the middle and left HV, were present, whereas the right HV was absent. The branches of

the HVs were readily recognizable. The morphological appearance and internal vascular structure of the liver indicated that the liver defect was in the right hepatic lobe.

In SG2 (−3.6SD, CS20), the liver was found only in the upper right side of the abdominal cavity. The surface of the liver was irregular, except for the cranial side, which contacted the right diaphragm (△ in Fig. 4A). The liver was separated into 2 portions, a main large unit on the right (a) and a small satellite unit on the left (b in Fig. 4A,B). The UV, DV, and PV systems were not detected within the liver (Fig. 4B). The 2 terminal HVs, namely, the right and middle/left HVs, were recognizable, whereas the branches of the HVs were poorly developed in the plane section. The UV was deviated to the right side at its entrance into the liver, and the plane sections showed no vascular structure within the liver. Instead, an abnormal vein was observed running along the right lateral surface of the liver and connecting with the common hepatic vein (CHV) (Fig. 4A caudal view). It was not determined whether this vein was the deviated UV and DV or a collateral vein. The stomach (St) was inverted and deviated ventrally and cranially between the 2 liver units (Fig. 4C). The pancreas was also deviated towards the caudal side of the stomach.

In SG3 (−3.0SD, CS21), the liver was located in the ventral part of the abdominal cavity and contacted the ventral abdominal wall but not the lateral abdominal wall or either side of the diaphragm (Fig. 5A,B). The surface of the liver was irregular on all sides, with a prominent projection on the right cranial surface (Fig. 5A). The liver was not herniated into the thoracic cavity, as the diaphragm was observed in the plane section (△ in Fig. 5B-b). The UV and PV systems in the liver were detected in the plane section (Fig. 5B-c-d). The UV was flattened transversely both at the entrance and intrahepatically, and the DV was also flattened (* in Fig. 5A). Of the PV systems, the PS and several main branches were recognizable but the sub-branches were not. The 3 terminal HVs, namely the right, middle, and left HVs, were observed. Branches of both the PV and HV systems were detected, although the connections to the main trunk were not confirmed. There was suspicion of gastroschisis (** in Fig. 5B-e).

In SG4 (−2.2SD, CS21), the liver was located in the middle of the abdominal cavity. The liver was divided into right and left sides cranially that fused caudally, leaving a sharp straight cleft on the median line of the abdominal side (Fig. 6A). The liver did not contact the abdominal wall in the vicinity of the cleft; a low-intensity area

was present between them (** in Fig. 6B). The surface of the liver was irregular except for the left ventral side, although the liver partially reached the abdominal wall and both sides of the diaphragm (△ in Fig. 6B). The UV was recognizable but flattened transversely both at its entrance into the liver and in its intrahepatic region, and then the DV was constricted (* in Fig. 6A). The PV system was also abnormal: the PS was visible, but its main branches and their sub-branches were only barely visible. The 2 terminal HVs, namely, the left and middle HVs, were present, whereas the right HV was detectable only as a bump on the CHV.

In SG5 (−2.8SD, CS21), the liver was located in the ventral part of the abdominal cavity, where it contacted the ventral abdominal wall and the left side of the diaphragm. The surface of the liver was irregular on all sides (Fig. 7A). The UV was recognizable as a trapezoid at its entrance into the liver and as flattened transversely in its intrahepatic region, whereas the diameter of the DV was within the reference range (* in Fig. 7A). The PV systems were barely visible in the plane section. The 3 terminal HVs, namely, the right, middle, and left HVs, were present, whereas their branches were hardly recognizable. The abnormality of the liver affects the locations of the other

internal organs, especially the stomach and duodenum (Fig. 7A). The stomach was deviated ventrally and cranially beneath the liver. The pyloric antrum was straight and ran vertically in the right ventral abdomen. Notably, the relative positions of the cardia and pylorus were not affected (Fig. 7A). The pancreas was not deviated (data not shown). The body wall was thin, with defects of the skin and the muscular layer (* in Fig. 7B-d). An area of high-intensity comparable to that of the liver was noted just beneath the abnormal body wall (** in Fig. 7B-d). The area was not connected to the liver and was not identified.

In SG7 (CS21), no liver was detected in any of the serial plane sections (Fig. 8A-a-c). The stomach was observed on the midsagittal line in the Th9 and Th10 transverse sections, indicating that the stomach had deviated cranially and ventrally. On the right side of the stomach, ligaments with high intensity were observed running from the diaphragm to the right abdominal wall (* in Fig. 8A-a-c). The diaphragm was apparent in these sections wall (△ in Fig. 8A-a-b). The duodenum was located in the right ventral part of the abdomen, and the pancreas deviated ventrally in the Th12 transverse section (Fig. 8A-c). The locations of all intrathoracic, retroperitoneal, and

intra-abdominal organs were reconstructed in 3 dimensions as shown in Figure 8B. The absence of the liver affected the locations of the other internal organs, especially the stomach, duodenum, and pancreas (Fig. 8B-b). The stomach was inverted. The pyloric antrum was straight and ran vertically in the right ventral quadrant. Notably, the relative positions of the cardia and pylorus were not affected (Fig. 8B-b). The pancreas originated from the duodenum, and its tail deviated ventrally.

Similar complications were detected in SG6 (CS21), which also had no detectable liver (data not shown).

Liver morphological structure in the embryos with a large liver

Abnormality of the liver was detected in 2 embryos at CS18 (LG5, LG6) (Figs. 9 and 10). No obvious abnormality of the morphology or internal vascular structures of the liver was detected by precise observations using PCT images in the remaining 6 cases despite a liver size of >2SD greater than the mean volume. Of the 2 LG embryos with morphological abnormality, 1 had only a liver abnormality and the other had a morphologically abnormal liver with complications in other organs as well.

In LG5 (+3.1SD, CS18), the liver was large in the cranial-caudal and transverse dimensions (Fig. 9A). The surface of the liver was smooth. Vascular structures such as the UV and DV were present within the liver but were ambiguous because of the high intensity of the images (Fig. 9B). The UV was recognizable as dilatated, whereas the diameter of the DV was within the reference range (Fig. 9B). The PV systems, that is, the PS and its main and sub-branches, were detected. The 3 terminal HVs, namely, the right, middle, and left HVs, were present, whereas their branches were not detected. In the PV and HV, dilatation of the venous lumen was observed in several locations.

In LG6 (+5.1SD, CS18), the liver was severely deformed (Fig. 10A). The liver was so large in the cranial-caudal dimension that it was seen to herniate into the thoracic cavity, and hypogenesis of the diaphragm was detected in the plane section (△ in Fig. 10A and Fig. 10B). The liver had bilateral hollows on the ventral surface that contacted the deformed abdominal wall. The internal structure of the liver was indistinct and in the plane section was almost homogenous, with relatively low intensity (Fig. 10B). No obvious histological structures such as vascular structures or lobules were detected. Severe complications including abnormality of the external appearance were noted in

this case. The locations of intrathoracic and intra-abdominal organs were reconstructed in 3 dimensions (Fig. 10A-Left lateral view). The bilateral lungs were hypogenetic; that is, the intensity of the mesenchyme around the lobar bronchi was low (Fig. 10B-a). The stomach was surrounded by the liver (Fig. 10B-c). The wall and lumen of the stomach were irregular (▲ in Fig.10B-c). The both atria of the heart were severely deformed.

Discussion

In the present study, the strategy of using a large embryo collection (Kyoto collection), from a MRI database and PXCT was proposed to be useful for elucidating the cause of spontaneous abortion and/or intrauterine death (Figure 1). Livers selected for their potentially abnormal embryos were screened for their volumes. The novel SLMs was revealed in externally normal embryos by detailed observation on MRM and PXCT. The cause of spontaneous abortion of externally normal embryos in the embryonic stage remains unknown in most cases (Shiota, 1991; O'Rahilly and Müller, 2001). The present study demonstrated that the proposed methods may reveal the cause of spontaneous abortions and/or intrauterine death.

The liver was selected as target organ for several reasons as follows: 1) For screening potentially abnormal embryos, standardized morphology and morphometry are required. The liver is well recognizable being the largest organ in the abdominal cavity, and its morphology and morphometry have been recently described (Hirose et al., 2012; Hamabe et al., 2013). The estimation of liver volume is possible, as 3-D morphology is relatively simple. Estimation of liver morphology is useful for evaluating not only the

liver itself but also the adjacent organs that affect the stage-specific morphology of the liver, as liver morphology is affected by adjacent organs. 2) The liver is one of the most important organs not only in the adult stage but also in the embryonic stage, which plays an important role in the development of functional organs (Lemaigre, 2009). The liver becomes a hematopoietic organ after 6 weeks (Migliaccio et al., 1986; Tavian et al., 2000) and then begins to metabolize biochemical materials important for development, such as albumin, bile, glycogen, and fetus-specific proteins, during the fetal period (Koga, 1971). Liver malformation may cause spontaneous abortion and/or intrauterine death. 3) Liver tissues are recognizable as high-signal intensities, and the internal structure of the liver (artery, vein, and portal vein) is also well recognizable on PXCT.

The SG may be subdivided according to defect type as follows: agenesis, hypogenesis, or lobe defect. All but one case with a lobe defect (SG1) may result in spontaneous abortion and/or intrauterine death due to liver failure. This case (SG1) can result in live birth without severe complications if the remaining liver can compensate for the function. The defect in this group may be similar or identical to congenital agenesis of the right liver, reported as a rare condition that is generally asymptomatic

(Iannelli et al., 2005). The diagnosis is made based on the absence of visualization of the right HV and right PV (and its branches), as well as dilatation of the right intrahepatic duct (Chou et al., 1998).

Embryos with extra-large livers were detected at a relatively high rate between CS14 and CS23 (3.5%, 41/1156). However, no obvious morphological abnormality was detected in all but 2 cases (LG5 and LG6) after reviewing MR and PXCT images. The defect in LG6 might lead to spontaneous abortion and/or intrauterine death, whereas that in LG5 can result in live birth, although congenital disease of the circulatory system and/or liver function might be present. We did not determine whether the large livers other than LG5 and LG6 had potential abnormalities that we could not detect by using the present method or whether the abnormal size was only a periodical phenomenon, that is, benign variation from the reference range for the developmental stage.

The SLMs in the present study were found only between CS18 and CS21. The detection rate of SLMs in the externally normal embryos between CS18 and CS21 was high at approximately 1.7%. One possible explanation for this observation is that

embryos with a SLMs may not survive past these stages because of liver failure. In several cases (SG4, LG6), the gestational age was older than that for normal embryos at the same stage, suggesting intrauterine growth retardation (data not shown).

In the present study, 2 methods, namely MRM and PXCT, were used for screening and precise internal observation, respectively (Matsuda et al., 2003; Yoneyama et al., 2011). Both of these imaging methods are noninvasive and nondestructive, which are important properties of modalities for analyzing scarce specimens such as human embryos. MRM is a powerful tool for precise 3-D measurement and observation of the external morphological structure of the liver (Matsuda et al., 2003). PXCT, in contrast, is a novel method for analysis of smaller objects and provides a resolution ≥ 18 μm/pixel (Yoneyama et al., 2011). This technique enables highly sensitive measurement with approximately >1,000-fold higher resolution than the conventional radiographic method, which uses absorption contrast. Work is ongoing to apply PXCT to the detection of pathological findings such as cancer tissues and amyloid plaques in brain tissue (Takeda et al., 2004; Noda-Saita et al., 2006). As shown in the Results section, the image resolution was high enough to show not only

the morphological structure of the internal organs but also the internal structure of the liver. These capabilities allowed the precise diagnosis of the pathology of each embryo without histological analysis. Sample size is one limitation of PXCT, which is applicable to embryos between CS15 and CS21. The other limitation is that a special facility (i.e., a radiographic imaging system) was required for acquisition of the PXCT images. The number of samples acquired in the present study was therefore limited.

The strategy of using a large embryo collection (Kyoto collection) from an MRM image database and PXCT revealed liver abnormalities in externally normal embryos. Other important organs such as the brain, heart, lungs, and skeleton may be next targets. For these organs, however, the standardized morphometry and morphology for routine screening and detailed observation was not established. The present study is a first step toward the elucidation of the causes of spontaneous abortion and/or intrauterine death in externally normal embryos, which has never previously been accomplished. The proposed methods will contribute to advance the field of fetal diagnosis and developmental anatomy.

Acknowledgments

We are deeply indebted to Associate Professor Kazuyuki Hyodo of Photon Factory for allowing us to use the synchrotron radiographic equipment at the BL-14C. We also thank President Kohei Shiota of Shiga University of medical science for providing the invaluable MR data.

Literature Cited

Chou C, Mak C, Lin M, Tzeng W, Chang J. 1998. CT of agenesis and atrophy of the right hepatic lobe. Abdom Imaging 23:603-607.

Hamabe Y, Hirose A, Yamada S, Uwabe C, Okada T, Togashi K, Takakuwa T. 2013. Morphology and morphometry of fetal liver at 16–26 weeks of gestation by magnetic resonance imaging: Comparison with embryonic liver at Carnegie stage 23. Hepatol Res *43:*639-647.

Hirose A, Nakashima T, Yamada S, Uwabe C, Kose K, Takakuwa T. 2012. Embryonic liver morphology and morphometry by magnetic resonance microscopic imaging. Anat Rec 295:51-59.

Iannelli A, Facchiano E, Fabiani P, Sejor E, Bernard J, Niezar E, Gugenheim J. 2005. Agenesis of the right liver: a difficult laparoscopic cholecystectomy. J Laparoendosc Adv Surg Tech 15:166-169.

Kaigai N, Nako A, Yamada S, Uwabe C, Kose K, Takakuwa T. 2014. Morphogenesis and Three - Dimensional Movement of the Stomach During the Human Embryonic Period. Anat Rec 297:791-797.

Kagurasho M, Yamada S, Uwabe C, Kose K, Takakuwa T. 2012. Movement of the external ear in human embryo. Head Face Med 8:2.

Kameda T, Yamada S, Uwabe C, Suganuma N. 2012. Digitization of clinical and epidemiological data from the Kyoto Collection of Human Embryos: maternal risk factors and embryonic malformations. Congenit Anom *52*:48-54.

Koga A. 1971. Morphogenesis of intrahepatic bile ducts of the human fetus. Z Anat Entwicklungsgesch 135:156-184.

Lemaigre FP. 2009. Mechanisms of liver development: concepts for understanding liver disorders and design of novel therapies. Gastroenterology 137:62-79.

Matsuda Y, Utsuzawa S, Kurimoto T, Haishi T, Yamazaki Y, Kose K, Anno I, Marutani M. 2003. Super-parallel MR microscope. Magn Reson Med 50:183-189.

Migliaccio G, Migliaccio AR, Petti S, Mavilio F, Russo G, Lazzaro D, Testa U, Marinucci M, Peschle C. 1986. Human embryonic hemopoiesis. Kinetics of progenitors and precursors underlying the yolk sac—liver transition. J Clin Invest 78:51-60.

Nakashima T, Hirose A, Yamada S, Uwabe C, Kose K, Takakuwa T. 2012. Morphometric analysis of the brain vesicles during the human embryonic period by magnetic resonance microscopic imaging. Congenit anom 52:55-58.

Nishimura H, Takano K, Tanimura T, Yasuda M. 1968. Normal and abnormal development of human embryos: first report of the analysis of 1,213 intact embryos. Teratology 1:281-290.

Nishimura H. 1975. Prenatal versus postnatal malformations based on the Japanese experience on induced abortions in the human being. In: Blandau RJ, ed. Aging gametes. Basel: S Karger AG. p.349 –368

Nishimura H, Tanimura T, Semba R, Uwabe C. Normal development of early human embryos: observation of 90 specimens at Carnegie stages 7 to 13. Teratology 1974;10(1):1-5.

O'Rahilly R, Müller F. 1987. Developmental stages in human embryos: including a revision of Streeter's Horizons and a survey of the Carnegie Collection. Washington, D.C.: Carnegie Institution of Washington. p. 239–251.

Noda-Saita K, Yoneyama A, Shitaka Y, Hirai Y, Terai K, Wu J, Takeda T, Hyodo K, Osakabe N, Yamaguchi T. 2006. Quantitative analysis of amyloid plaques in a mouse model of Alzheimer's disease by phase-contrast X-ray computed tomography. Neuroscience 138:1205-1213.

O'Rahilly R, Müller F. 2001. Stages, age, measurements, growth, and external form including the face. In: O'Rahilly R, Müller F, editors. Human embryology and teratology. 3rd ed. New York: Wiley-Liss, Inc. p. 87-113.

Shiota K. 1991. Development and intrauterine fate of normal and abnormal human conceptuses. Congenit Anom 31:67-80.

Shiota K, Yamada S, Nakatsu-Komatsu T, Uwabe C, Kose K, Matsuda Y, Haishi T, Mizuta S, Matsuda T. 2007. Visualization of human prenatal development by magnetic resonance imaging (MRI). Am J Med Genet A 143A:3121-3126.

Shiraishi N, Nakashima T, Yamada S, Uwabe C, Kose K, Takakuwa T. 2013. Morphogenesis of Lateral Choroid Plexus During Human Embryonic Period. Anat Rec 296:692-700.

Takeda T, Yoneyama A, Wu J, Lwin TT, Tsuchiya Y, Hyodo K. 2004. In vivo imaging of cancer implanted in nude mice by two-crystal interferometer-based phase-contrast X-ray computed tomography. Jpn J Appl Phys 43:L1144.

Tavian M, Hallais M, Péault B. 1999. Emergence of intraembryonic hematopoietic precursors in the pre-liver human embryo. Development 126:793-803.

Yamada S, Samtani RR, Lee ES, Lockett E, Uwabe C, Shiota K, Anderson SA, Lo CW. 2010. Developmental atlas of the early first trimester human embryo. Dev Dyn 239:1585-1595.

Yoneyama A, Amino N, Mori M, Kudoh M, Takeda T, Hyodo K, Hirai Y. 2006. Non-invasive and time-resolved observation of tumors implanted in living mice by using phase-contrast X-ray computed tomography. Jpn J Appl Phys 45:1864.

Yoneyama A, Yamada S, Takeda T. 2011. Fine biomedical imaging using X-ray phase-sensitive technique. In: Dr. Gaetano Gargiulo, editor. Advanced biomedical engineering. Rijeka: InTech. p 107-128.

Figure Legends

Figure 1 Protocol for detecting latent abnormal embryos that result in spontaneous abortion and/or intrauterine death.

Figure 2. Screening of the human embryos with potential liver abnormalities.

(A) The estimated liver volume for 1,156 embryos. Liver volume was calculated as described in the Materials and Methods. The data for each Carnegie stage (CS) are shown as the mean ± 2 standard deviations (SD) mm^3.

(B) Distribution of the human embryos selected after screening using the estimated liver volume. Number of embryos with an extra-large (white □) or extra-small (black ■) liver.

Figure 3. The PXCT 3-D reconstructed images and the representative 2-D liver sectional images of the extra-small liver group (SG)1 (−2.9SD, CS20) and of a normal

control for comparison.

(A) The ventral and left lateral 3-D views. The entrance of the umbilical vein (UV) (●) into and exit of the common hepatic vein (HV) (○) from the liver are shown as anatomical reference points. The HV was hidden on the dorsal side of the 3-D reconstructed image. The direction of the blood flow is indicated by the black arrows. The plane corresponding to the coronal section in Fig. 3B is indicated as a dashed line. The UV was severely flattened transversely and constricted (* in Left lateral view). The scale bar indicates 1 mm. DV, ductus venosus.

(B) The coronal and transverse sectional images. The internal vascular structure, UV (→), portal vein (△), DV (▲), and HV (▲) were recognizable. The asterisk (*) in coronal section indicates the malforming of the internal structure of the liver (Li). The UV was severely flattened transversely. Es, esophagus; St, stomach.

Figure 4. The PXCT 3-D reconstructed images and the representative 2-D liver sectional images of the extra-small liver group (SG)2 (−3.6SD, CS20) and of a normal

control for comparison.

(A) The ventral and caudal 3-D views. The entrance of the umbilical vein (●) into and exit of the common hepatic vein (HV) (○) from the liver are shown as anatomical reference points. The HV was hidden on the dorsal side of the 3-D reconstructed image. The orientation is indicated as ventral (V) and dorsal (D) in caudal view. The direction of the blood flow is indicated by black arrows. The surface of the liver was smooth on the cranial side, which contacted the right side of the diaphragm (△). The liver was separated into 2 parts, a main large unit on the right (a) and a small satellite unit on the left (b). The scale bar indicates 1 mm.

(B) The transverse liver sectional images at Th7 from SG2 and at Th9 from normal control (CS20). Ad, adrenal gland; In, intestine; Li, liver; Lu, lung; St, stomach.

(C) The ventral 3-D views demonstrated the relationship between the liver and stomach (St). The scale bar indicates 1 mm.

Figure 5. The PXCT 3-D reconstructed images and the representative 2-D liver

sectional images of the extra-small liver group (SG)3 (−3.0SD, CS21).

(A) The ventral and left lateral 3-D views. The entrance of the umbilical vein (UV) (●) into and exit of the common hepatic vein (HV) (○) from the liver are shown as anatomical reference points. The HV was hidden on the dorsal side of the 3-D reconstructed image. The direction of the blood flow is indicated by arrows. The plane corresponding to the coronal section in Fig. 5B is indicated as a dashed line. The UV and ductus venosus (DV) were flattened (* in Left lateral view). The scale bar indicates 1 mm.

(B) The coronal, sagittal, and transverse sectional images. The UV was flattened (→) (a). There was a low-intensity area (*) between the liver (Li) and left diaphragm (△), indicating that the diaphragm had developed (b). The UV (→), portal vein (△), and DV (▲) were indicated (c,d). There was suspicion of gastroschisis (**) (e). Ad, adrenal gland; He, heart; Lu, lung; Mt, metanephros; St, stomach.

Figure 6. The PXCT 3-D reconstructed images and the representative 2-D liver

sectional images of the extra-small liver group (SG)4 (−2.2SD, CS21).

(A) The ventral and left lateral 3-D views. The entrance of the umbilical vein (UV) (●) into and exit of the common hepatic vein (HV) (○) from the liver are shown as anatomical reference points. The HV was hidden on the dorsal side of the 3-D reconstructed image. The direction of the blood flow is indicated by the black arrows. The liver was divided into right and left sides at the cranial surface. The UV was flattened and the ductus venosus (DV) was constricted (*). The scale bar indicates 1 mm.

(B) The sagittal and transverse sectional images. There was a low-intensity area (*) between the liver (Li) and left diaphragm (△), indicating that the diaphragm had developed. The sides of the liver were separate at Th10 (**). Ad, adrenal gland; He, heart; Lu, lung; Mt, metanephros.

Figure 7. The PXCT 3-D reconstructed images and the representative 2-D liver sectional images of the extra-small liver group (SG)5 (−2.8SD, CS21).

(A) The ventral and left lateral 3-D views. The entrance of the umbilical vein (UV) (●) into and exit of the common hepatic vein (HV) (○) from the liver are shown as anatomical reference points. The HV was hidden on the dorsal side of the 3-D reconstructed image. The direction of the blood flow is indicated by the arrows. The UV was flattened (*). The scale bar indicates 1 mm. cardia (▲), and pylorus (▲). Du, duodenum; DV, ductus venosus; St, stomach.

(B) The sagittal and transverse sectional images. There was a low-intensity area (*) between the liver (Li) and right diaphragm (△), indicating that the diaphragm had developed (a). The UV (→), HV (▲), and DV (▲) were indicated (b,c). The body wall was thin, with defects of the skin and the muscular layer (*). An area of high-intensity (**) comparable to that of the liver (Li) was noted just beneath the abnormal body wall (d). Ad, adrenal gland; Du, duodenum; Es, esophagus; He, heart; In, intestine; Lu, lung; Ms, mesonephros; St, stomach.

Figure 8. The PXCT 3-D reconstructed images and the representative 2-D liver

sectional images of the extra-small liver group (SG)7 (no liver, CS21) and a control specimen for comparison.

(A) Serial transverse sections. The asterisk indicates the high-intensity area present in the right abdominal space (a-c). Pancreas (▲), diaphragm (△), and hepatic vein (▲). Ad, adrenal gland; Du, duodenum; Ge, genital ridge; In, intestine; Li, liver; Lu, lung; Mt, metanephros; St, stomach.

(B) The 3-D reconstructed images, demonstrating the complications accompanying the agenesis of the liver. The scale bar indicates 1 mm. Cardia (▲) and pylorus (▲). He, heart; Ms, mesonephros; Pa, pancreas.

Figure 9. The PXCT 3-D reconstructed images and the representative 2-D liver sectional images of the extra-large liver group (LG)5 (+3.1SD, CS18) and of a normal control for comparison.

(A) The Vntral and left lateral 3-D views. The entrance of the umbilical vein (UV) (●) into and exit of the common hepatic vein (HV) (○) from the liver are shown as

anatomical reference points. The HV was hidden on the dorsal side of the 3-D reconstructed image. The direction of the blood flow is indicated by the arrows. The plane corresponding to the coronal section in Fig. 9B is indicated as a dashed line. The scale bar indicates 1 mm. DV, ductus venosus.

(B) The coronal and transverse sectional images. The UV (→), portal vein (△), DV (▲), and HV (▲) were indicated. Li, liver; Tc, thoracic cavity.

Figure 10. The PXCT 3-D reconstructed images and the representative 2-D liver sectional images of the extra-large liver group (LG)6 (+5.1SD, CS18).

(A) The ventral and left lateral 3-D views. The entrance of the UV (●) into the liver is shown as anatomical reference point. The symbol △ indicates the herniation of the liver (Li) into the thoracic cavity that resulted in confusion of the border between the liver and the lung (Lu). The scale bar indicates 1 mm. He, heart; St, stomach.

(B) The sagittal and transverse sectional images. The symbol ▲ indicates the wall and lumen of the stomach were irregular. Ms, mesonephros.

Table

Table 1A. Summary of the liver findings in the series of liver malformations

case	CS	CRL (mm)	liver volume (SD[a])	(sub)group	Internal vascular structure				related figure No.
					UV	DV	PV	HV	
SG1	20	13.7	-2.9	defect of the lobe	flattened	(-)	(-)	(-)	S1
SG2	20	13.4	-3.6	hypogenetic	n.d.[b]	n.d.	n.d.	hypogenetic	S2
SG3	21	19.7	-3.0	hypogenetic	flattened	flattened	hypogenetic	(-)	S3
SG4	21	18.9	-2.2	hypogenetic	flattened	constricted	hypogenetic	hypogenetic	S4
SG5	21	21.1	-2.8	hypogenetic	flattened[c]	(-)	n.d.	hypogenetic	S5
SG6	21	16.6	-3.3	agenetic	n.d.	n.d.	n.d.	n.d.	S6
SG7	21	18.0	-3.3	agenetic	n.d.	n.d.	n.d.	n.d.	F5
LG5	18	13.7	+3.1	extra-large	dilatated	(-)	dilatated	dilatated	S7
LG6	18	15.0	+5.1	extra-large	n.d.	n.d.	n.d.	n.d.	F6

CS, Carnegie stage; CRL, crown-rump length; UV, umbilical vein; DV, ductus venosus; PV, portal vein; HV, hepatic vein; (-), within the reference range for the developmental stage; n.d., not detected; F, Figure; S, Supplementary Figure.

[a]SD is the number of standard deviations from the mean estimated liver volume (Ve) for the developmental stage.

[b]The UV was deviated to the right side at its entrance into the liver.

[c]The UV was recognizable as a trapezoid at its entrance into the liver.

Table

Table 1B. Summary of the complications in organs other than the liver in the series of liver malformations

case	CS	stomach	intestine (mid-gut)	pancreas	heart	lung	mesonephros / genital ridge	abdominal wall	related figure No.
SG2	20	deviated	deviated	deviated	(-)	(-)	(-)	(-)	S2
SG3	21	(-)	(-)	(-)	(-)	(-)	(-)	gastroschisis[a]	S3
SG5	21	deviated	deviated	(-)	(-)	(-)	(-)	gastroschisis[a]	S5
SG6	21	deviated	deviated	deviated	(-)	(-)	agenetic	(-)	S6
SG7	21	deviated	deviated	deviated	(-)	(-)	(-)	(-)	F5
LG6	18	irregular[b]	(-)	(-)	deformed	hypogenetic	(-)	(-)	F6

(-), within the reference range for the developmental stage; F, Figure; S, Supplementary Figure.

[a]There was suspicion of gastroschisis.

[b]The wall and lumen of the stomach were irregular.

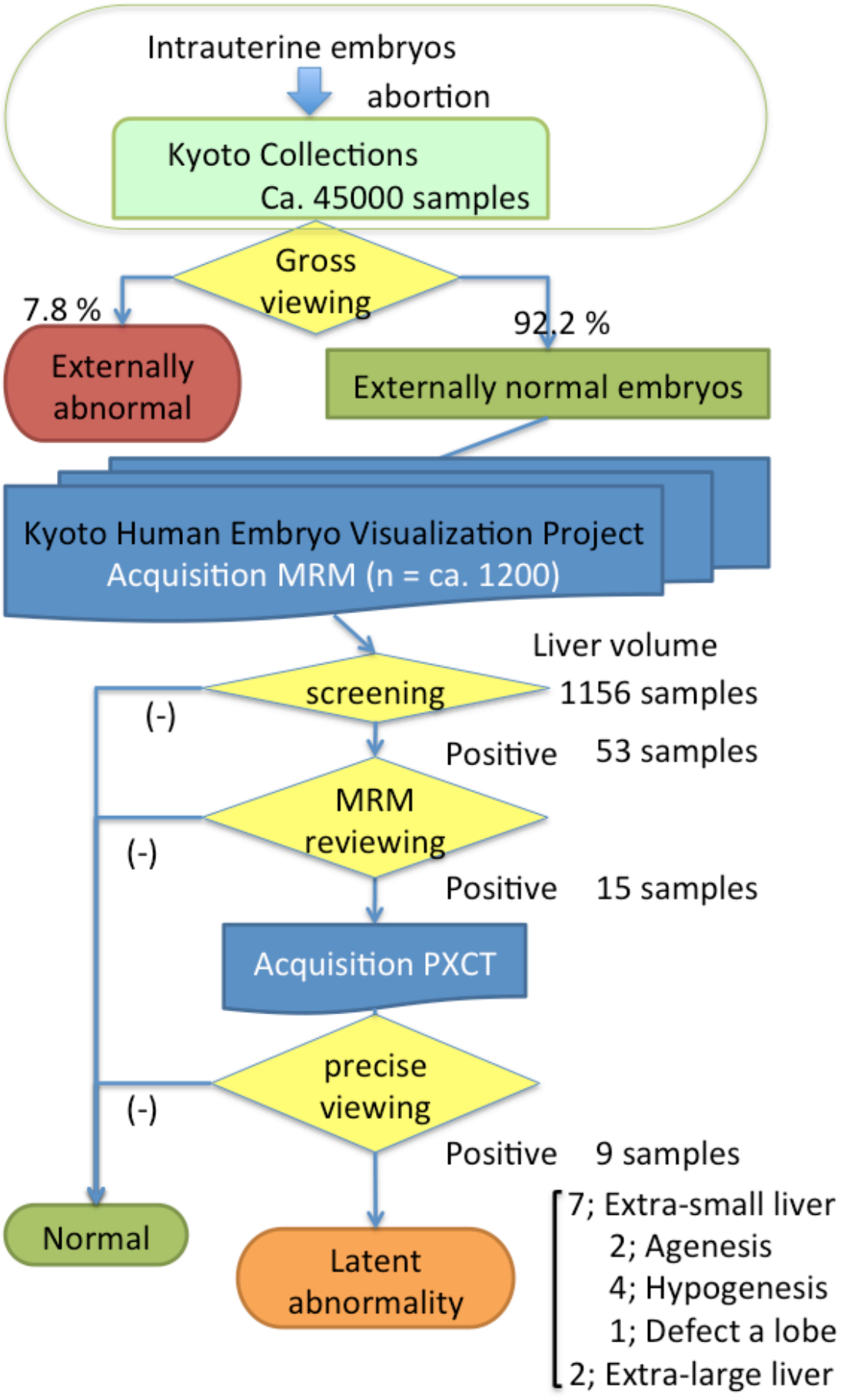
Intrauterine embryos
abortion
Kyoto Collections
Ca. 45000 samples
Gross viewing
7.8 %
92.2 %
Externally abnormal
Externally normal embryos
Kyoto Human Embryo Visualization Project
Acquisition MRM (n = ca. 1200)
Liver volume
screening
1156 samples
(-)
Positive
53 samples
MRM reviewing
(-)
Positive
15 samples
Acquisition PXCT
precise viewing
(-)
Positive
9 samples
Normal
Latent abnormality
7; Extra-small liver
2; Agenesis
4; Hypogenesis
1; Defect a lobe
2; Extra-large liver

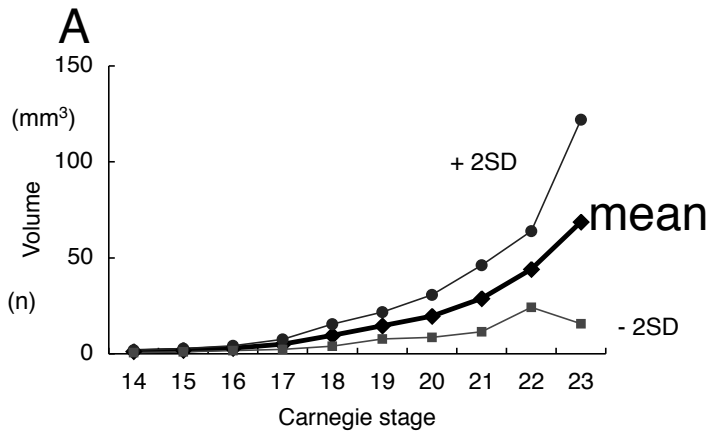
A
150
(mm3)
100
Volume
50
(n)
0
+ 2SD
mean
- 2SD
14 15 16 17 18 19 20 21 22 23
Carnegie stage

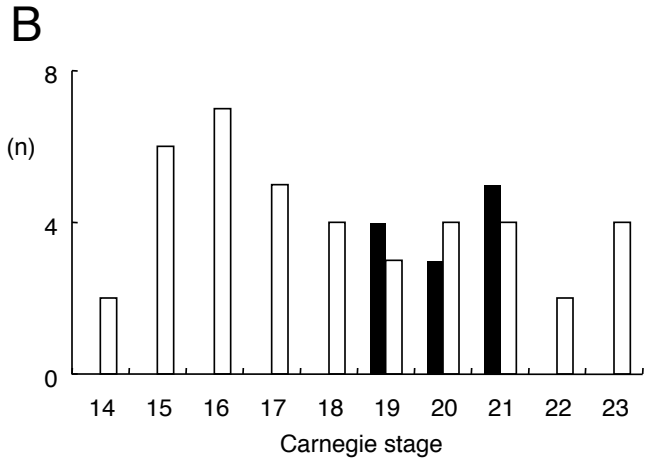
B
8
(n)
4
0
14 15 16 17 18 19 20 21 22 23
Carnegie stage

Fig. 2

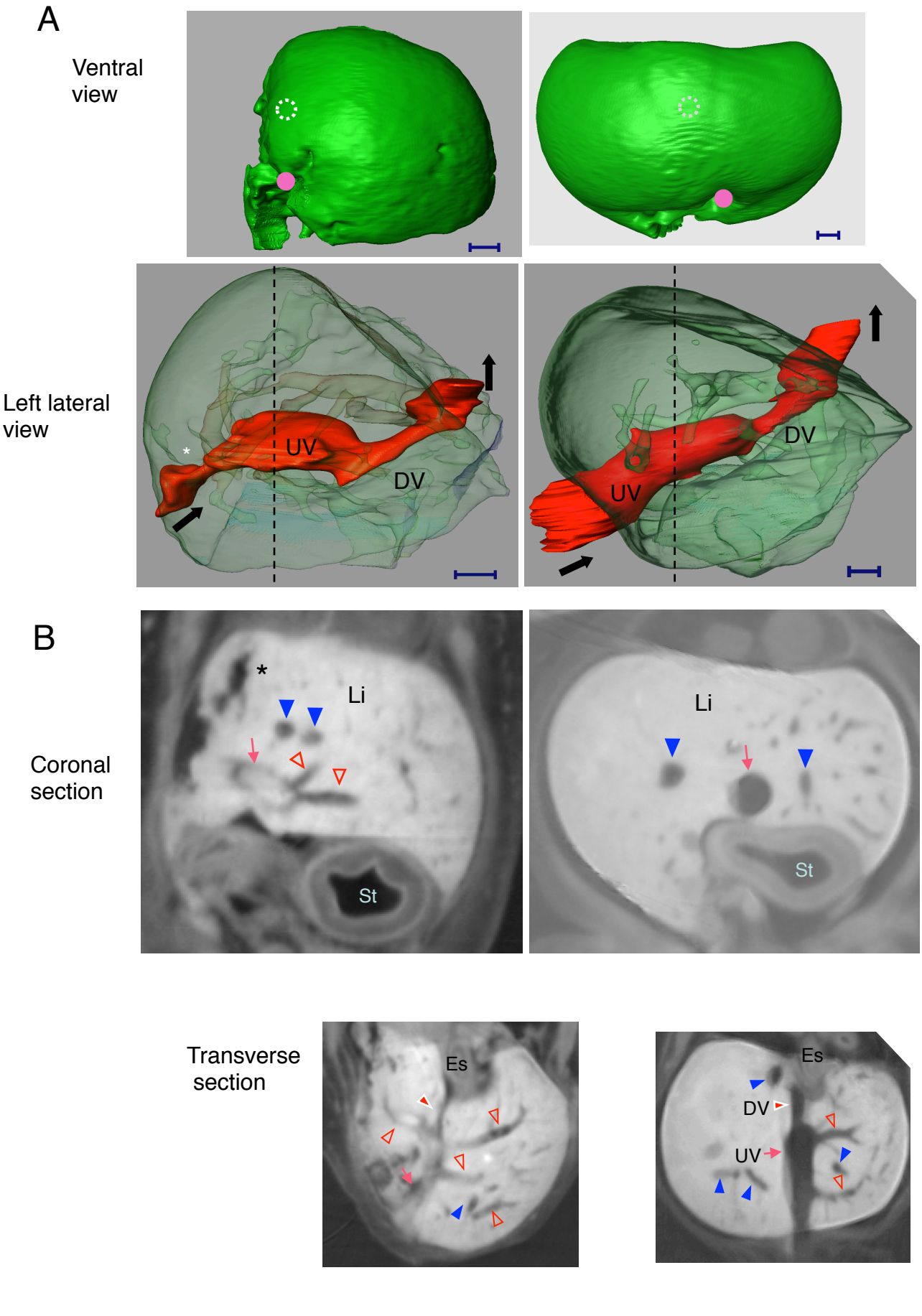
SG1
Control (CS20)
A
Ventral view
Left lateral view
UV
DV
UV
DV
*
B
Coronal section
*
Li
St
Li
St
Transverse section
Es
Es
DV
UV

Fig. 3 SG1

A

SG2

Ventral view

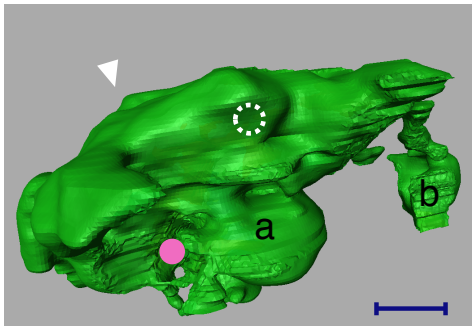

Caudal view

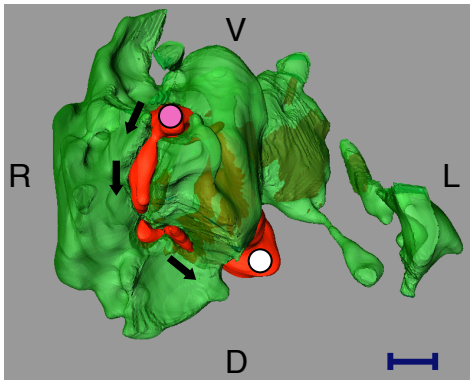

SG2

Control

B

Transverse section

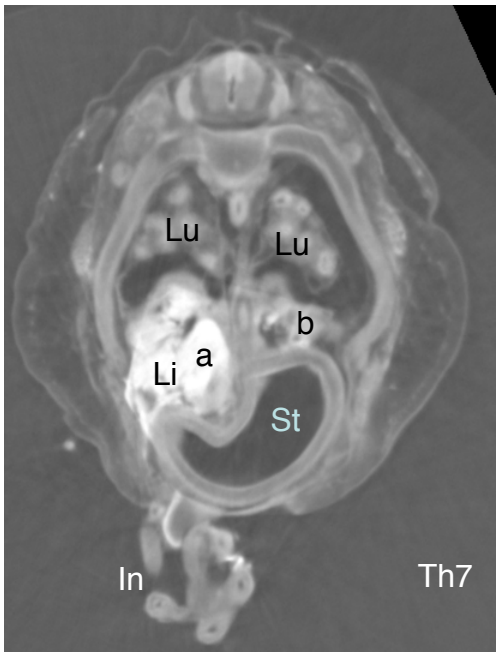

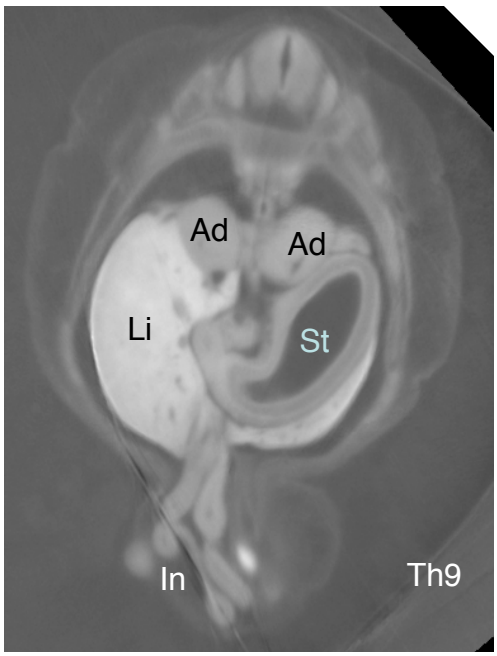

C

Ventral View with stomach

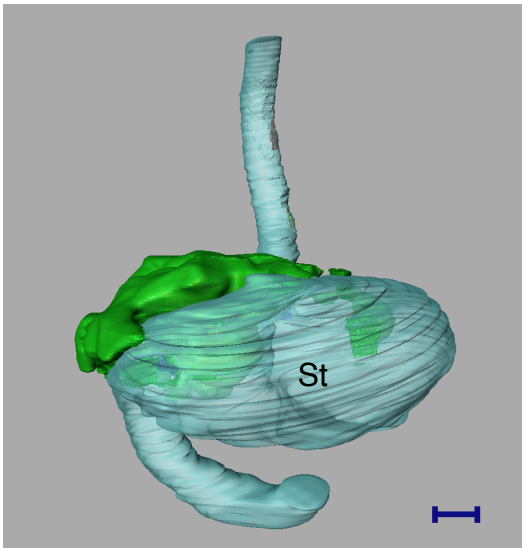

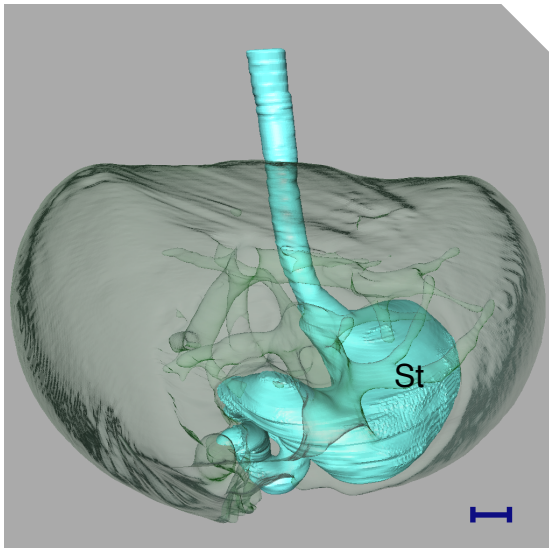

Fig4

A

Ventral view

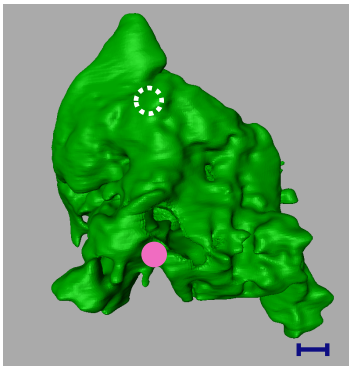

Left lateral view

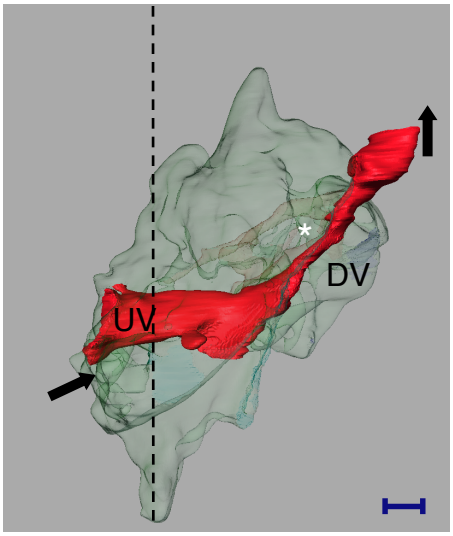

B

Coronal section

Sagittal section

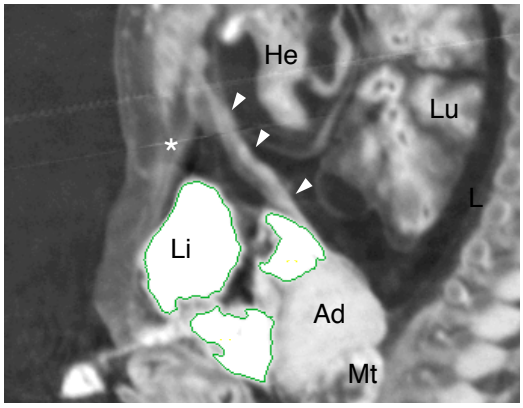

Transverse section

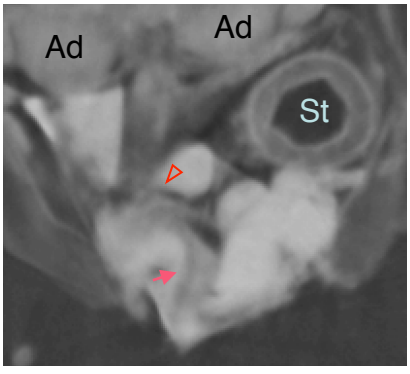

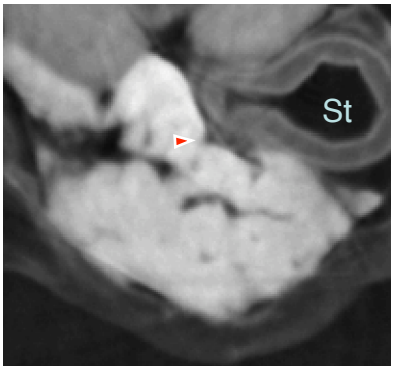

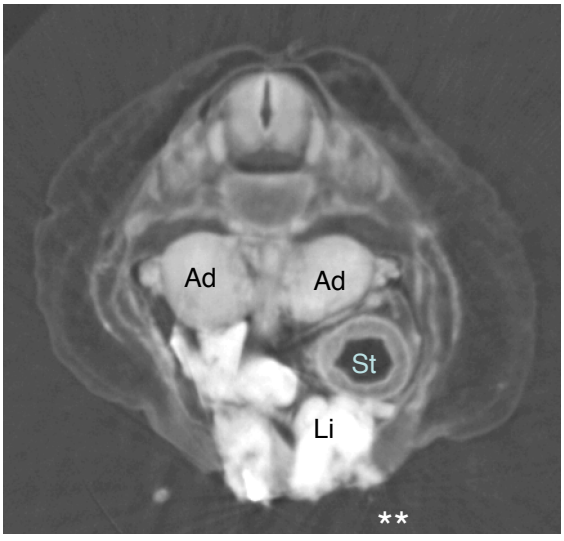

Fig. 5

SG3

A

Ventral view

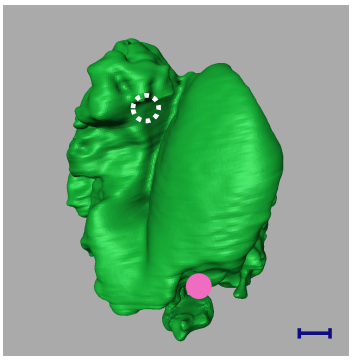

Left lateral view

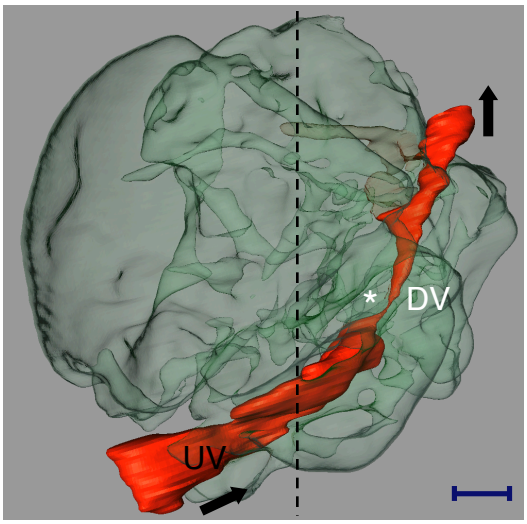

B

Coronal section

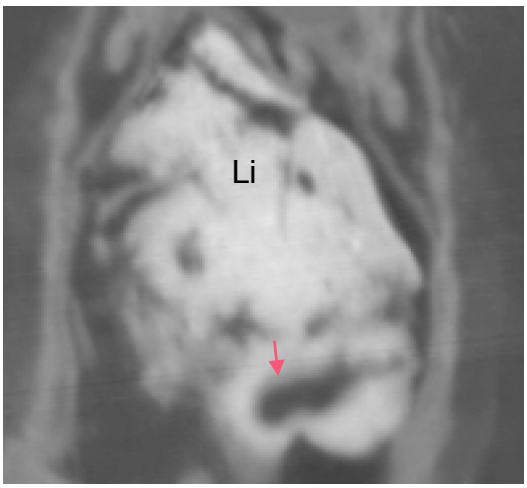

Sagittal section

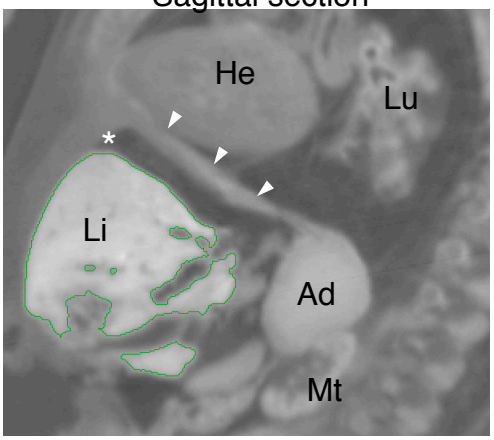

Transverse section

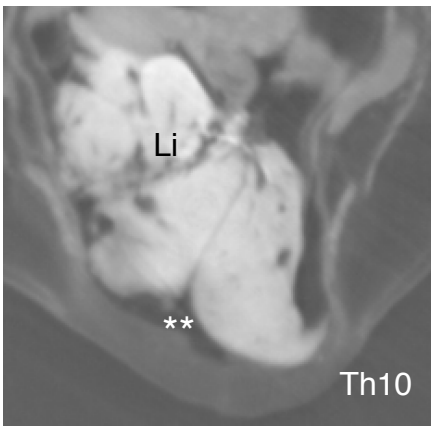

A

Ventral view

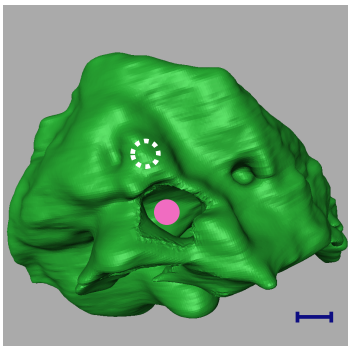

Left lateral view

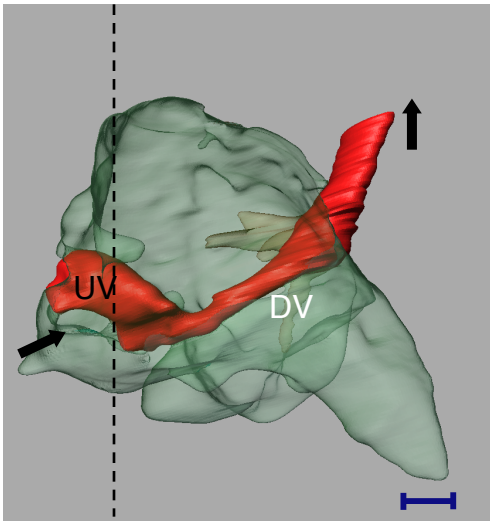

Ventral view
with stomach

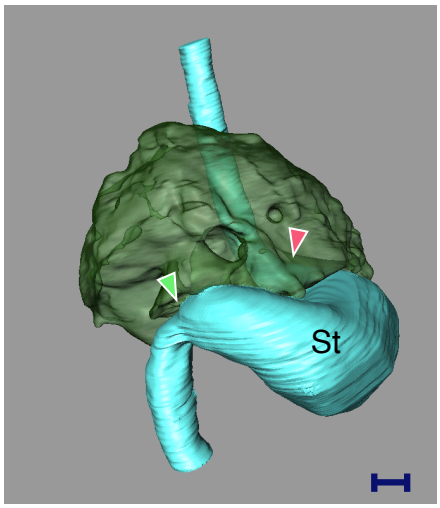

Sagittal section

B

Coronal section

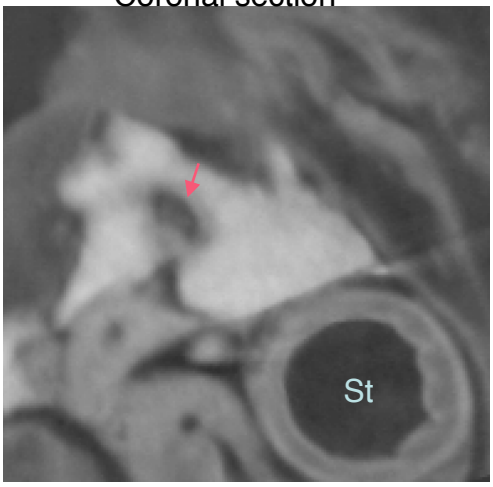

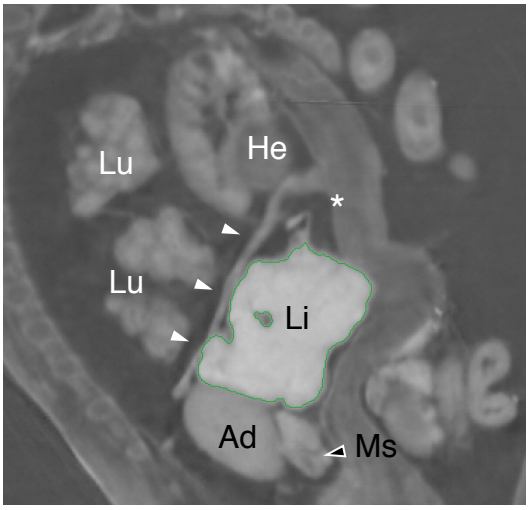

Transverse section

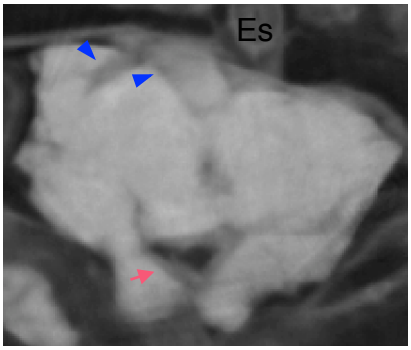

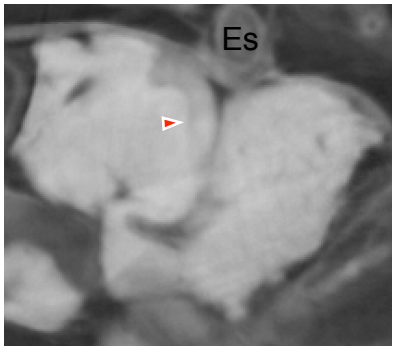

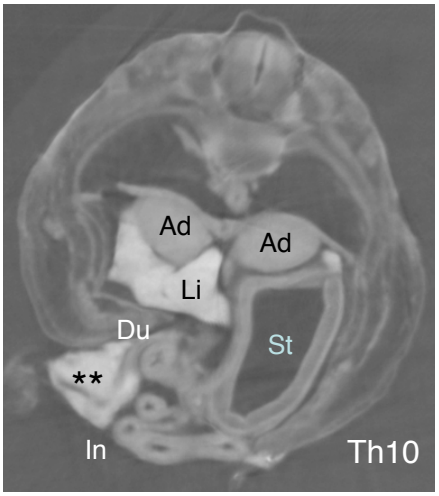

Fig. 7 SG5

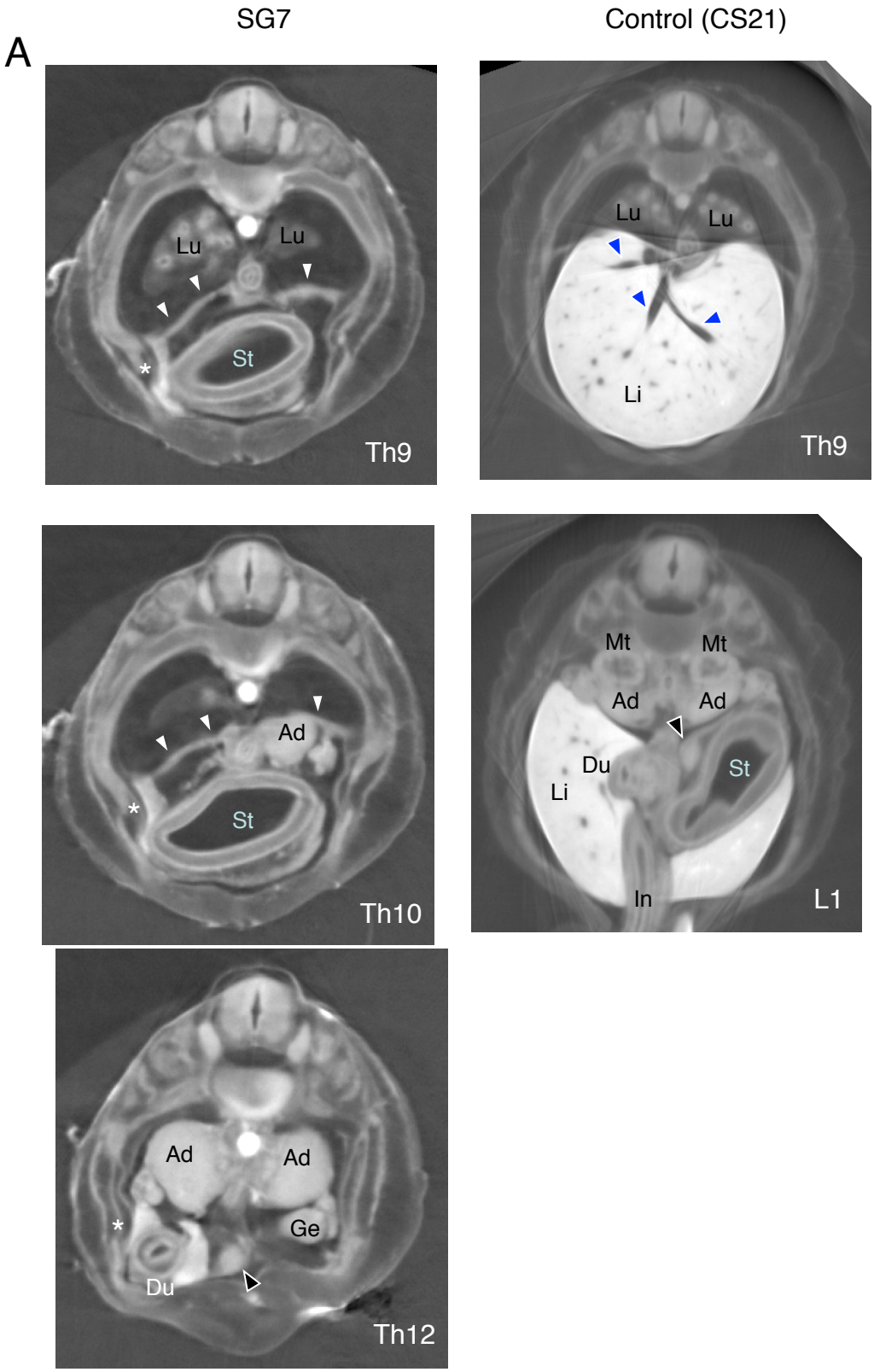
A
SG7
Control (CS21)
Lu
Lu
St
Th9
Lu
Lu
Li
Th9
Ad
St
Th10
Mt
Mt
Ad
Ad
Du
St
Li
In
L1
Ad
Ad
Ge
Du
Th12

Fig. 8

SG7

B

left anterior
oblique view

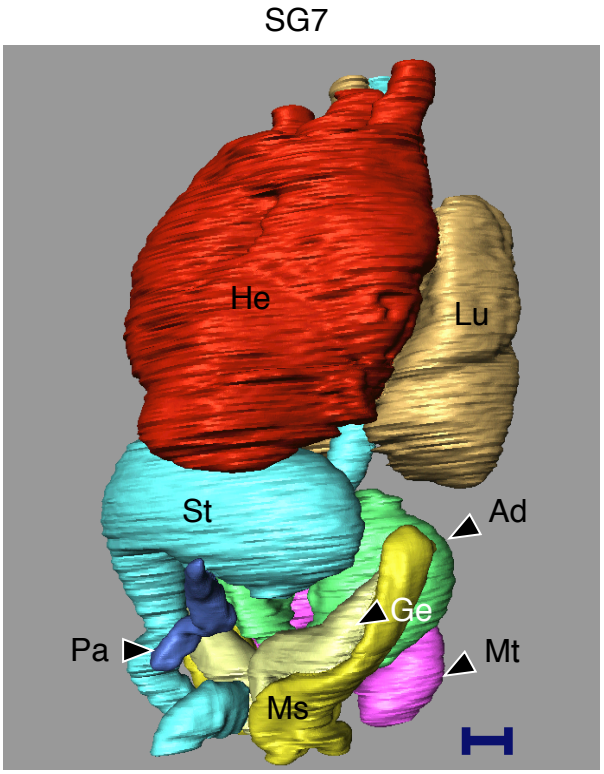

stomach, duodenum,
and pancreas

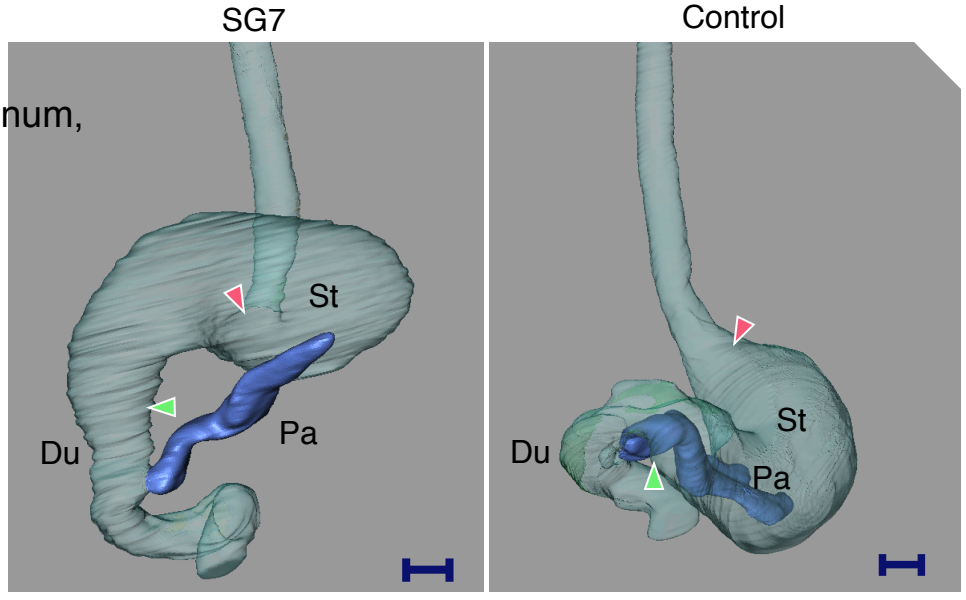

Fig. 8B

SG7

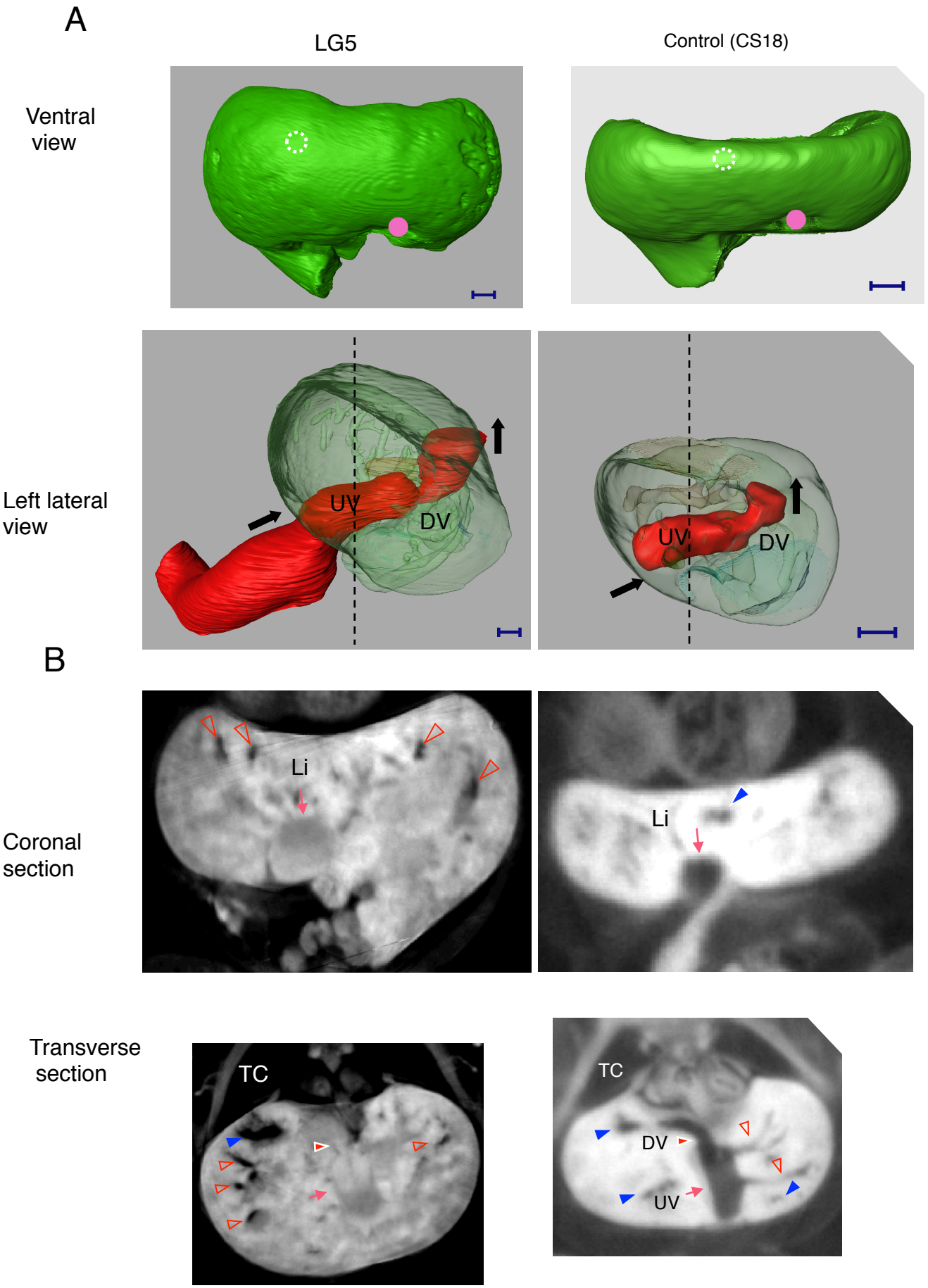
A
LG5
Control (CS18)
Ventral view
Left lateral view
UV
DV
UV
DV
B
Coronal section
Li
Li
Transverse section
TC
TC
DV
UV

Fig.9

A

Ventral view

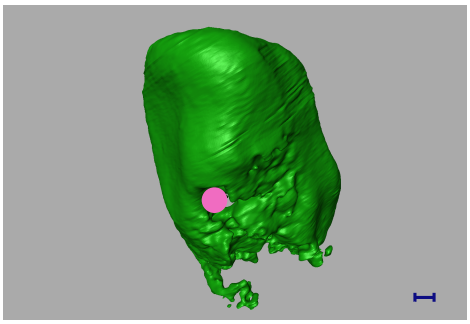

Left lateral view

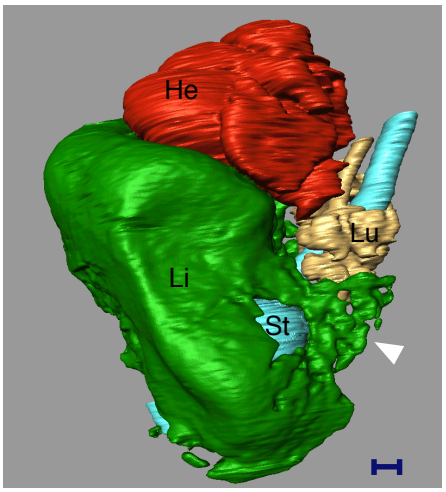

Dorsal view

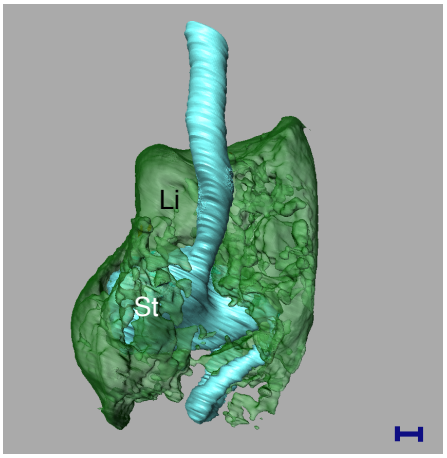

B

Sagittal section

Transverse section

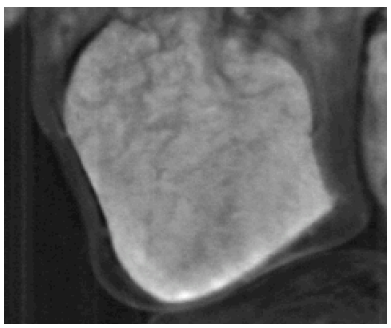

Transverse section

Fig. 10

LG6